Ultrasonics Sonochemistry 82 (2022) 105909

Contents lists available at ScienceDirect

Ultrasonics Sonochemistry

journal homepage: www.elsevier.com/locate/ultson

Experimental and numerical investigation of the effect of ultrasound on the growth kinetics of zeolite A

Ruben M. Dewes [a], Heidy Ramirez Mendoza [b], Mafalda Valdez Lancinha Pereira [b], Cécile Lutz [b], Tom Van Gerven [a,*]

[a] Department of Chemical Engineering, KU Leuven, Celestijnenlaan 200F, 3001 Leuven, Belgium
[b] Service Adsorption, ARKEMA, Groupement de Recherche de Lacq, Lacq, France

ARTICLE INFO

Keywords:
Zeolite A
Ultrasound
Modelling
Kinetics

ABSTRACT

Ultrasound is a promising technology for the improvement of zeolite production, due to its beneficial effects on mass transfer and nucleation. However, a broad understanding of the sonication parameters that influence the growth of zeolites most is still lacking. In the present work, zeolite A was synthesized and the kinetic model of Gualtieri was used to obtain information about the crystallization parameters. The effect of the sonication power and duration on the relative crystallinity and particle size distribution were investigated using a Langevin-type transducer operating at 40 kHz. The experimental data shows that ultrasound has a significant effect on the nucleation and growth. With that, a reduction of up to 40 % of the initial synthesis time can be achieved. Additionally, a narrower particle size distribution is achieved when ultrasound is used during the zeolite A synthesis.

1. Introduction

With the increasing demand of more sustainability, ultrasound offers the opportunity to enhance production processes. In conventional crystallization processes ultrasound already showed its beneficial properties, where an acceleration of the crystallization could be achieved [1,2]. The most common theories behind this phenomenon are based on the occurrence of cavitation bubbles in the liquid. Cavitation bubbles are believed to act as nucleation sites, from which a heterogeneous nucleation is initiated [3]. Wohlgemuth et al. investigated the effect of gas bubbles induced into a batch reactor to clarify the effect of cavitation during crystallization [4]. By the induction of gas bubbles a reduction of the metastable zone width was achieved, comparable to the effect that is observable with ultrasound. Another hypothesis suggests, that during the expansion of the cavitation bubble solvent evaporates into the bubble, which leads to a higher supersaturation around the bubble surface and hence, to an induction for nucleation [5].

In contrary to the conventional crystallization processes, the formation of zeolites is more complex. Zeolites consist of a structured framework of alumina and silica tetrahedra [6]. The crystallization usually starts from an amorphous aluminosilicate gel, where a breakage and restructuring of the initial Si-O-Si and Al-O-Al bonds occurs, until a nucleus with a structured zeolite framework is built [7]. Due to the required restructuring, the synthesis of zeolites is a time consuming process, where the formation of the final product can take from hours [8] to days [9]. Within the last years research about different zeolite types showed that ultrasound can have a positive effect on their growth, which reduced the total synthesis time significantly [10–15]. Phenomena like acoustic streaming or enhanced nucleation rates are suspected to be responsible for the beneficial effect of ultrasound [16]. Yet, a full understanding of the effects of sonication parameters during the synthesis is not available.

Therefore, in the current work the effect of ultrasound is investigated in a batch setup for various sonication and synthesis times, as well as the sonication power to obtain an overview about how the synthesis of zeolite A is affected. For this purpose, a model developed by Gualtieri is used, where an estimation about the nucleation and growth can be drawn.

2. Materials & methods

2.1. Materials

Starting materials for the zeolite A synthesis were sodium meta-

* Corresponding author.
E-mail address: tom.vangerven@kuleuven.be (T.V. Gerven).

https://doi.org/10.1016/j.ultsonch.2022.105909
Received 29 October 2021; Received in revised form 31 December 2021; Accepted 4 January 2022
Available online 15 January 2022

silicate nonahydrate (⩾98 wt%, Sigma Aldrich), sodium aluminate (50–56 wt% Al_2O_3, 37–45 wt% Na_2O, Sigma Aldrich) and sodium hydroxide (⩾99 wt%, Fisher Scientific).

For the terephthalic acid dosimetry dibasic sodium phosphate (⩾99 wt%, Sigma Aldrich), monobasic potassium phosphate (⩾99 wt%, Sigma Aldrich), sodium hydroxide (⩾99 wt%, Fisher Scientific) and terephthalic acid (98 wt%, Sigma Aldrich) were used. As a reference for a calibration curve 2-hydroxyterephthalic acid (97 wt%, Sigma Aldrich) was used.

The dihydrate of calcium chloride (⩾99 wt%, Sigma Aldrich) was used for the ion exchange of zeolite A for the BET measurements. All chemicals were used as purchased.

2.2. Sample preparation

Zeolite A was synthesized based on the procedure by Thompson and Huber [17] from a sodium metasilicate nonahydrate and sodium aluminate solution. Both solutions were prepared with 60 g of deionized water and 0.3615 g of sodium hydroxide. For the solution that acts as silica source, 15.48 g of sodium metasilicate nonahydrate was added. In the second solution 8.258 g of sodium aluminate was dissolved. The clear solutions were poured into a custom-made cylindrical double-walled glass reactor, which was heated to 80 °C and stirred at 750 rpm with an axial stirrer. On the bottom of the reactor a transducer (STEMiNC, SMBLTF20W120) with a glued glass plate on its top is attached to seal the reactor and to introduce ultrasound into the system, see Fig. 1. Experiments were conducted under silent conditions as a reference to experiments that were performed under sonication at a frequency of 40 kHz for the kinetic studies. Input powers of 10 W, 20 W, 30 W, 40 W and 50 W were used for a duration of 10 min and the corresponding power densities (0.08 W/cm^3, 0.17 W/cm^3, 0.25 W/cm^3, 0.33 W/cm^3 and 0.42 W/cm^3) were calculated by dividing the calorimetric power P_{cal} with the volume of the liquid. For the calculation of the calorimetric power ultrasound was applied for 10 min and the change of temperature was recorded. With the temperature T, the time t, the heat capacity of the solvent c_P and the mass of the solvent m, the calorimetric power can be calculated as [3]

$$P_{cal} = \frac{dT}{dt} c_P m \quad (1)$$

Starting from a reported synthesis time of 60 min, the duration was increased by 30 min until no change in relative crystallinity was observed for unsonicated and sonicated experiments. Each data point obtained represents here an individual experiment for which the whole content of the reactor was used. Additionally, experiments with a fixed power and a varying sonication time between 10–40 min were performed. Due to reaching the lifetime expectancy of the used transducer, a supplementary transducer (UltrasonicsWorld, MPI-7850D-20_40_60H) was used and a power of 33 W (0.33 W/cm^3) appeared to be suitable to reproduce the results obtained before with a power of 30 W. As a higher calorimetric power is required with the new transducer to obtain comparable results to the initial one, it appears that optimal conditions are dependent on the type of transducer used. At the end of the reaction the obtained zeolite suspension was filtered at 80 °C using a Merck Millipore PVDF membrane with a pore size of 0.22 µm and dried overnight at 80 °C.

2.3. Characterization

To determine the phase composition of the synthesized zeolite, X-ray diffraction (XRD) analysis was performed with a Bruker D2 Phaser (Cu Kα radiation) in a range between 5–50 °. The sample holder for the XRD was filled completely with each individual zeolite A sample and the surface was smoothed before it was inserted into the device. With the obtained XRD diffractogram an integration of the zeolite A peaks was performed and the background substracted. The relative crystallinity was calculated as the ratio between the peak surface area of a produced sample and the sample produced with the highest degree of crystallinity of each crystallization curve, which follows the normalization procedure described in [18].

The analysis of the morphology was conducted with a Jeol JSM-6010LV scanning electron microscope between 10–20 kV, with a Pd coating for 20 s.

With a Malvern Mastersizer 3000 the particle size distribution was

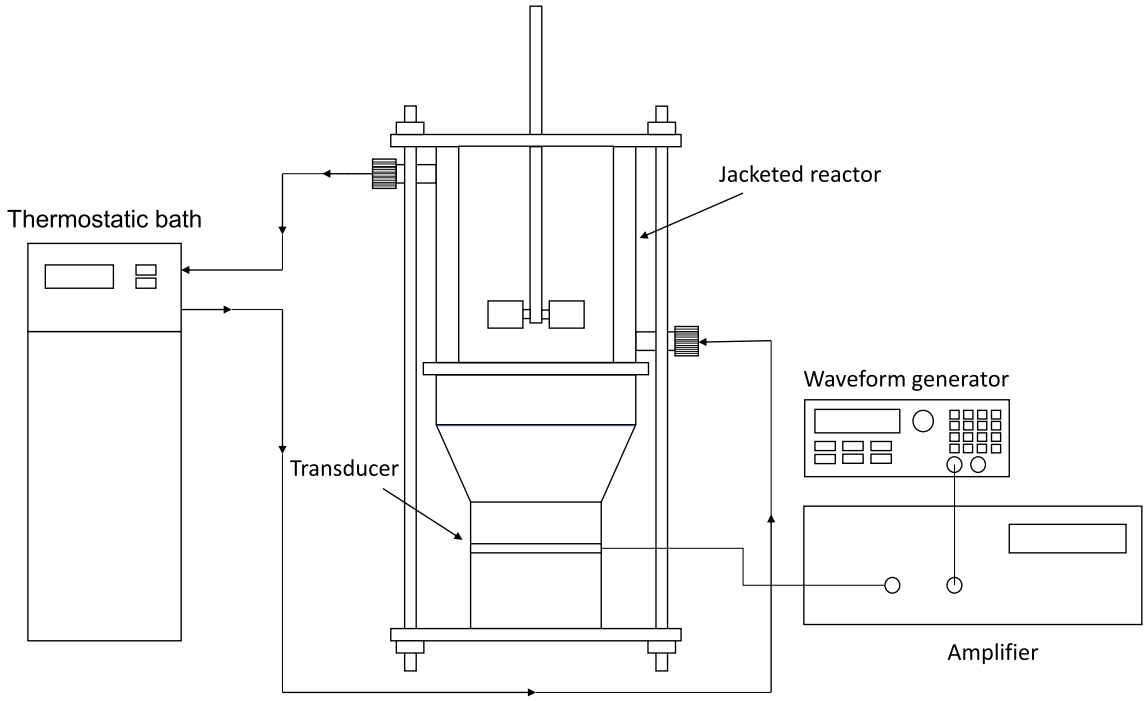

Fig. 1. Experimental setup for the synthesis of zeolite A in a double-walled glass reactor with an attached transducer on the bottom for the sonication of the reaction liquid.

determined, using a Hydro EV dispersing unit operated with a stirring speed of 2400 rpm. As dispersing medium water was chosen with an obscuration limit between 5–15 %. Due to the relatively high amount of sample required for the Hydro EV dispersing unit, a low variability of results is achieved. Thus, the error of the measurements is beyond the detection limit and is not shown in the corresponding tables.

For the terephthalic acid dosimetry a buffer solution with a pH of 7.4 was prepared according to the procedure described in [19,20]. Concentrations of 2 mM terephthalic acid, 5 mM sodium hydroxide, 4.4 mM dibasic potassium phosphate, 7 mM monobasic sodium phosphate were used for the buffer. As solvent ultrapure Milli-Q water from a Sartorius-Stedim Arium 611 DI water purification system was used. Temperatures of 25 ± 2 °C, 40 ± 2 °C, 60 ± 2 °C and 80 ± 2 °C were used with a period of sonication of in total 30 min. The ultrasound power for the experiments was varied in between 10 W, 20 W and 30 W and was kept constant over the whole period of each experiment. As the physico-chemical properties of the solution can have an effect on the maximum power applied by a transducer, 30 W was the highest power that could be realized for the terephthalic acid dosimetry. In total two repetitions were performed for each data point to obtain an estimation of the standard deviation of the experiment. As the product of the reaction of terephthalic acid with an OH-radical is 2-hydroxyterephthalic acid, a calibration curve of 2-hydroxyterephthalic acid was created, using a spectrofluorometer (Edinburgh Instruments FS900). For the fluorescence measurements an excitation wavelength of 312 nm and an emission maximum of 425 nm were used.

As a preparation step for the BET-measurements 1 g of each investigated zeolite A sample was dispersed in a 0.5 M calcium chloride solution of 200 mL to obtain the Ca-exchanged form of zeolite A. To ensure sufficient time for a complete ion exchange, the suspension was left over night. Following the ion exchange, the samples were filtered using a Merck Millipore PVDF membrane with a pore size of 0.22 µm, washed three times with 200 mL of deionized water and dried overnight at 60 °C. As activation program for the BET-measurements, a heating ramp of 3 °C/min to a final temperature of 200 °C was used and held for 12 h. Following this, N_2 was used to obtain the adsorption/desorption isotherms using a Micromeritics 3Flex adsorption analyzer. For an estimation of the micropore volume the t-plot method was used.

2.4. Modelling

To model the reaction kinetics the approach introduced by Gualtieri [18] was used. It is based on the assumptions that the crystal growth is not constant, it takes place in 1–3 dimensions, growth is symmetrical and that the nucleation can either be homogeneous, heterogeneous or autocatalytic in clear solutions or only heterogeneous or autocatalytic in dense solutions [18].

As a nucleation term Eq. 2 was used, where N is the total number of nuclei, t is the time (min) and a (min) and b (min) are fitting parameters.

$$N = \frac{1}{1 + \exp\left\{-\left(\frac{t-a}{b}\right)\right\}} \tag{2}$$

With Eq. 3 the growth process is described, including a growth and Gaussian expression. Here, x is the number of diffraction-observable crystals, k_g (min^{-1}) the growth rate constant and n the dimension of growth.

$$x = 1 - \exp[-(k_g t)^n] \tag{3}$$

Combining Eq. 2 and 3 delivers the final kinetic equation:

$$\alpha = \frac{1}{1 + \exp\left\{-\left(\frac{t-a}{b}\right)\right\}} \cdot \{1 - \exp[-(k_g t)^n]\} \tag{4}$$

The experimental data obtained for the kinetic curve was used to fit the parameters a,b, and k_g, using `lsqnonlin` in MATLAB R2018b. From the parameter a the nucleation rate constant can be calculated as $k_n = 1/a$. With the obtained parameter b an indication of the type of nucleation that is occurring is given. For $b \lesssim 15$ the nucleation is assumed to be heterogeneous, for $b \approx 20$ homogeneous and for $b > 20$ autocatalytic. These boundaries were obtained from Gualtieri [18] by fitting experimental data to an approximation introduced by Katović et al. [21].

3. Results & discussion

In Fig. 2 the experimental and modelling results of the crystallization curves of zeolite A are shown. The slowest crystallization occurs for the zeolite synthesis without any ultrasound used. Using ultrasound with only a power of 10 W, reduces the crystallization time already by at least 60 min. Increasing the power to 30 W leads to the fastest growth kinetics, where a detectable growth starts already after 60 min. Beyond this point crystallization occurs slower again for powers of 40 W and 50 W, yet, a significant difference to the unsonicated case is still present.

To obtain an understanding about the reduction of crystallization speed with increased power, the radical yield can be measured to get indirectly an insight in the characteristics of cavitation under the experimental conditions of the zeolite synthesis. In Fig. 3 a drop of radicals formed is present after a certain sonication power is exceeded. For a temperature of 25 °C the drop occurs after a sonication power of 20 W is exceeded, whereas for 40 °C and 60 °C the drop occurs already after a sonication power of 10 W. Increasing the power, leads to a larger number of cavitation bubbles being formed. After a certain threshold of cavitation bubbles is exceeded, scattering and absorption of the sound wave can occur by the bubbles [22,23]. As a result, the occurrence of cavitation is restricted to the vicinity of the transducer surface and with it the active zones in the reactor [24]. As the temperature is closer to the boiling point of water for 40 °C, 60 °C and 80 °C, the intensity of the cavitation bubble collapse is reduced, due to the higher content of vapour in the formed bubbles, which cushions the bubble implosion [25]. This leads to the steady decrease of radical yield measured with increasing temperature. Additionally, the higher volume of the cavitation bubbles, caused by the increase of vapour content, leads to an earlier drop of radical yield for 40 °C and 60 °C, compared to 25 °C. At a temperature of 80 °C a drop in radical yield does not occur, as the radical formation is already highly reduced by the cushioning effect mentioned above. In terms of the synthesis of zeolite A, these results indicate that the reduced efficiency in the crystallization process for sonicated conditions with powers above 30 W can be caused by the drop in efficiency

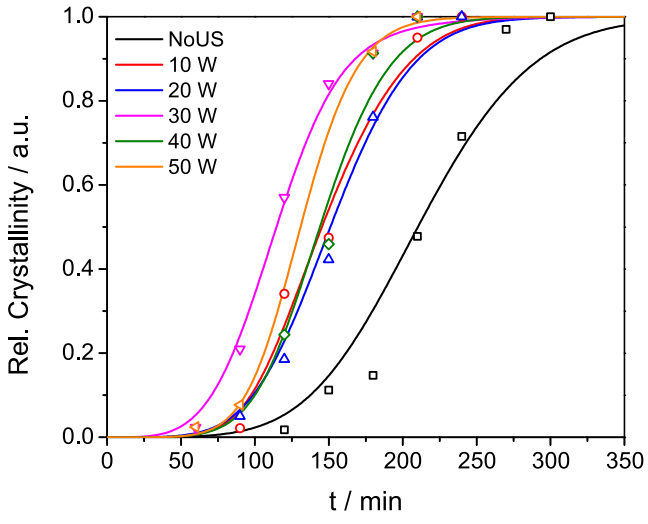

Fig. 2. Experimental and model and data obtained by the model of Gualtieri for the crystallization curves of zeolite A synthesized at 80 °C without ultrasound and under sonicated conditions with 10 W, 20 W, 30 W, 40 W and 50 W at 40 kHz for 10 min.

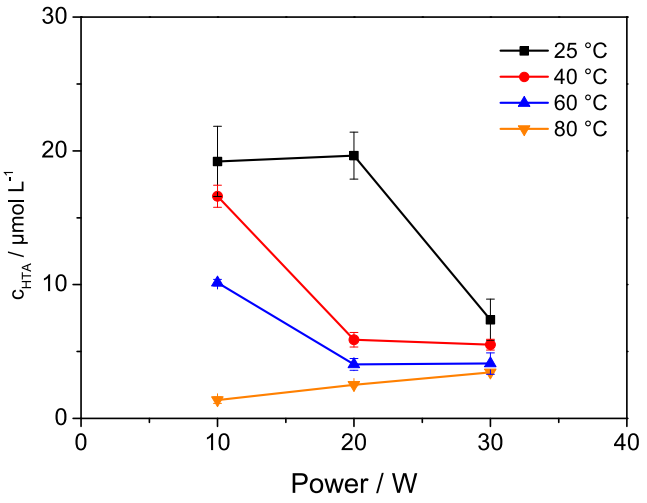

Fig. 3. Concentration of 2-hydroxyterephthalic acid formed by the reaction of terephthalic acid with OH-radicals, that are formed during the collapse of cavitation bubbles. A power of 10 W, 20 W and 30 W was applied under sonicated conditions for a duration of 30 min.

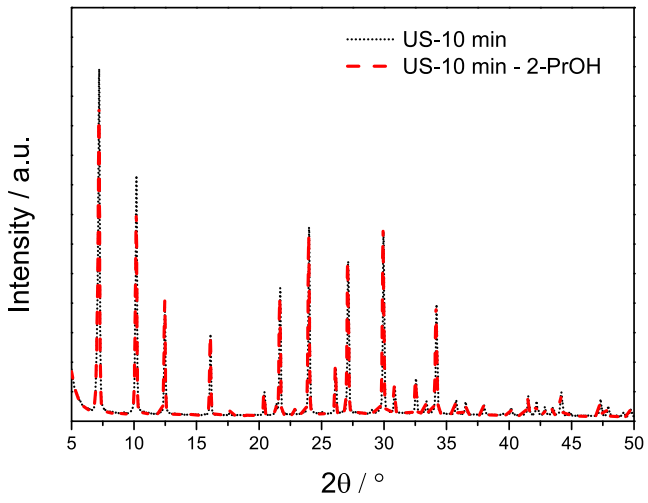

Fig. 4. XRD-diffractograms of zeolite A produced at 80 °C with the usage ultrasound for 10 min and a calorimetric power of 0.33 W/cm^3 and produced under the same conditions with 2 mL of additional 2-PrOH as radical scavenger.

of ultrasound, due to high cavitation formation. Even if the synthesis temperature of zeolite A is 80 °C, where no drop of radical yield is observed, it has to be considered that the boiling point of the reactive mixture is increased by the electrolyte solution, formed by the reactants. Thus, the cushioning effect on the cavitation bubble implosion is reduced and a drop in ultrasonic efficiency is assumed to occur for powers above 30 W. With the drop in ultrasonic efficiency and the above mentioned restriction of cavitation formation in the vicinity of the transducer surface, the area in which the cavitation bubbles can act as nucleation site is reduced. Hence, a deceleration of the zeolite A crystallization process occurs.

In total, a reduction of at least 30 % of the synthesis time can be achieved by using 10 min of ultrasound. One effect that ultrasound promotes is an enhanced mass transfer [26]. Collapsing cavitation bubbles that occur within the liquid cause an increased mixing within the reaction medium [11]. Within the modelling results, the enhanced mixing properties can be observed by the increase of the growth rate constant k_g, shown in Table 1. Another beneficial effect of ultrasound described in literature is the formation of radicals, due to the collapse of cavitation bubbles. It is described by Feng et al. that those radicals promote the depolymerization of Si-O-Si bonds of the synthesis gel [27]. The main effect is attributed to be on the nucleation stage, where the activation energy for the formation of new Si-O-Si bonds is lowered. Thus, the nucleation formation is promoted and the zeolite crystallization accelerated. With the aid of an added radical scavenger, in this case 2-propanol, the contribution of radicals to the process can be determined. As shown in Fig. 4, the addition of 2 mL of 2-propanol leads to a slight decrease in peak intensity. In total, this equals a decrease of integrated peak area of 9 %, see Table 2. However, despite the usage of a radical scavenger, a highly crystalline sample is produced. Thus, additional effects introduced by ultrasound have to play a major role. Here,

Table 1
Fitting data obtained by the model of Gualtieri with the experimental data for the zeolite A synthesis at 80 °C without ultrasound and sonication with 10 W, 20 W, 30 W, 40 W and 50 W at 40 kHz for 10 min.

	NoUS	10 W	20 W	30 W	40 W	50 W
k_g / min^{-1}	0.0048	0.0072	0.0065	0.0094	0.0071	0.0087
k_n / min^{-1}	0.0064	0.0089	0.0096	0.0118	0.0086	0.0084
b / min	44.32	33.23	30.23	34.41	23.99	20.67
R^2	0.9452	0.9787	0.9752	0.9880	0.9425	0.9838

Table 2
Integrated area of the zeolite A peaks obtained from the XRD-diffractograms for samples produced at 80 °C with the usage of ultrasound for 10 min and a calorimetric power of 0.33 W/cm^3 and produced under the same conditions with 2 mL of additional 2-PrOH as radical scavenger.

Sample	Integrated Area/ a.u.
US-10 min	10325
US-10 min – 2-PrOH	9388

cavitation bubbles acting as a nucleation site themselves can have a contribution [14]. A comparison of the predicted nucleation rate constants k_n shows, that the nucleation rate constant nearly doubles when ultrasound is used with a power of 30 W. Furthermore, with the supposedly prediction of the type of nucleation through the parameter b, an autocatalytic nucleation is estimated for all cases. As described by Mintova et al. nucleation of zeolite A starts with the nuclei formation within the amorphous gel, with the solution mass transfer being the growth limiting step [28]. Over time, those nuclei formed are getting released into the liquid phase, due to the dissolution of the gel, from which the crystalline phase starts to grow. As a result of the consumption of alumina and silica species for the growth of the released nuclei, the dissolution of the amorphous phase and thus, the release of further nuclei is accelerated over time. This leads to an 'explosive' rate of nuclei released, which indicates the autocatalytic stage [21]. Even if b is predicting this type of nucleation for all cases, a decrease of the value is observed with increasing sonication power, with nearly shifting towards a heterogeneous nucleation for a sonication power of 50 W. This indicates, that ultrasound promotes a quick release of nuclei from the gel phase. However, it has to be considered that those are pure numerical values that might not accurately reflect the true nature of nucleation.

In Fig. 5 the particle size distributions of the fully crystalline samples produced without ultrasound or with ultrasound for 10 min at 40 kHz and a power between 10–50 W are shown. Unsonicated zeolite A is showing a broader particle size distribution with larger particles than the sonicated cases, see Table 3. Ultrasound leads to a more narrow particle size distribution in all cases that appears to be similar except for a sonication power of 40 W. With the increasing number of nuclei induced by ultrasound, less silica/alumina species are available for each single nucleus, which restricts the size that can be achieved. Additionally, with the shorter synthesis time required for the sonicated samples less time is available for zeolite A to grow to a larger size.

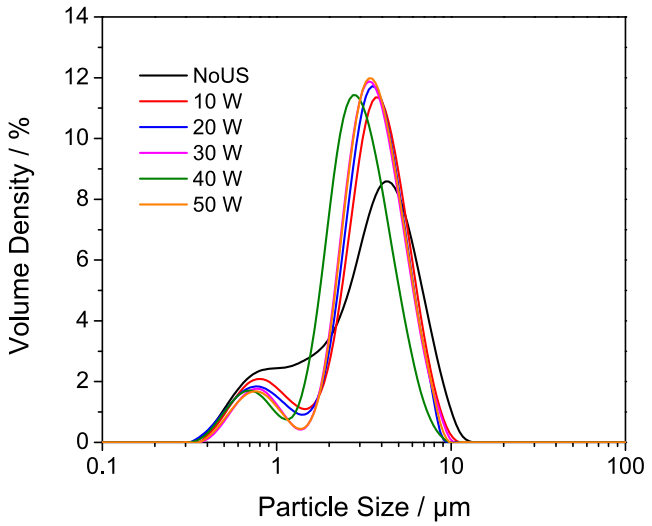

Fig. 5. Particle size distributions of zeolite A synthesized at 80 °C without ultrasound and sonication with 10 W, 20 W, 30 W, 40 W and 50 W at 40 kHz for 10 min.

Table 3
Measured values for d_{10}, d_{50} and d_{90} for zeolite A synthesized at 80 °C without ultrasound and with sonication using a power of 10 W, 20 W, 30 W, 40 W and 50 W at 40 kHz for 10 min. Measurement errors are not shown, due to them being beyond the detection limit of the device.

P_{son} / W	d_{10} /µm	d_{50} /µm	d_{90} /µm
0	0.94	3.68	7.20
10	1.02	3.75	6.43
20	1.04	3.62	6.12
30	1.31	3.61	6.19
40	1.23	2.98	5.23
50	1.36	3.63	6.17

The differences in particle size can also be observed by SEM, as shown in Fig. 6. The sonicated sample mainly shows zeolite A particles of the same size, whereas large differences in particle size are present for the unsonicated sample. With the homogeneous particle size for the sonicated case, it could indicate that ultrasound promotes most nuclei to form at the beginning of the synthesis. In contrary, the large variety of particle size in the conventional synthesis might be a result of a continuous formation of nuclei or release of nuclei from the gel phase during the whole synthesis process. On the image of the sonicated sample it appears that only one population of zeolite A is present, whereas in the laser diffraction measurements two populations are observed. Here, it has to be considered that images taken via SEM are only a qualitative analytical method. As the majority of the particle volume is located at around the larger size, smaller particles can be shadowed by larger ones. As smaller particles are visible on the surface of larger particles, it is evident that this smaller population exists and that it is not an artifact of the fitting routine used by the Malvern Mastersizer 3000.

A further effect that can be observed is a difference in the quantity of N_2 adsorbed during BET-measurements. As it can be seen in Fig. 7 a higher quantity of N_2 is adsorbed for zeolite A prepared with ultrasound, compared to zeolite A prepared without. The usage of ultrasound leads to an increase of the BET surface area from 594.5 m^2/g for zeolite A produced by the conventional method to 669.6 m^2/g for zeolite A produced with ultrasound. Moreover, the micropore volume increases by 0.03 cm^3/g through the usage of ultrasound, as it is shown in Table 4.

Increasing the sonication time leads to a further decrease of the time required to achieve full crystallinity, see Fig. 8. According to the model data, shown in Table 5, the nucleation rate constant increases from a sonication time of 10 min to 20 min and no significant changes are obtained by a longer usage of ultrasound. This indicates that no further improvement on the nucleation is achieved with longer sonication times. In contrary, a continuous slight increase of the growth rate constant can be observed by prolonged usage of ultrasound. Here, two

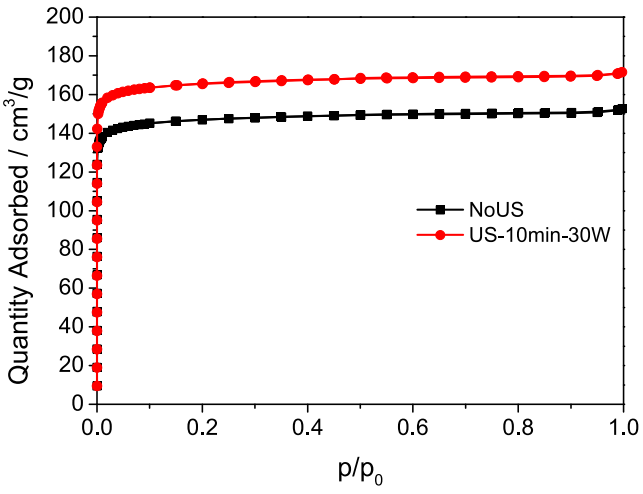

Fig. 7. BET isotherms for the adsorption/desorption of N_2 with zeolite A produced without ultrasound at 80 °C with a synthesis time of 5 h and zeolite A produced with ultrasound for 10 min with a power of 30 W at a frequency of 40 kHz and a synthesis time of 3.5 h.

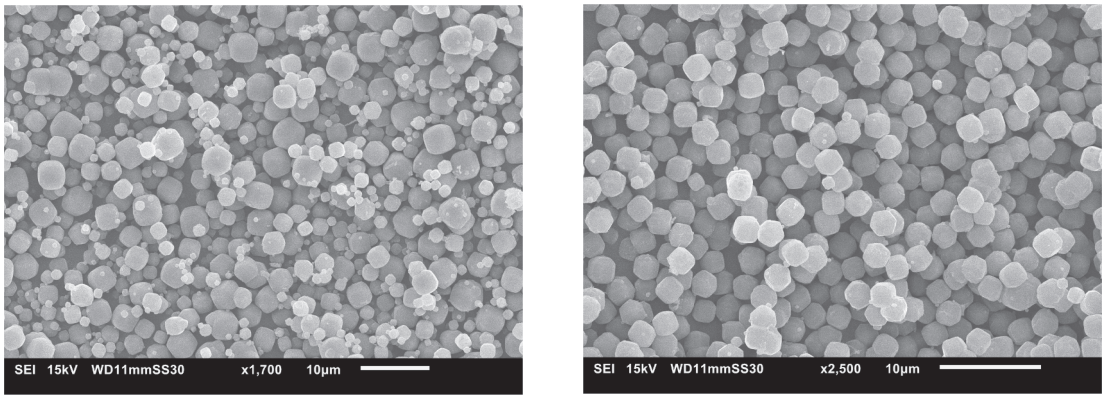

(a) (b)

Fig. 6. SEM-images of zeolite A synthesized at 80 °C without ultrasound (a) and with ultrasound at 40 kHz and a power of 30 W (b).

Table 4
BET surface area and micropore volume of zeolite A synthesized without ultrasound at 80 °C with a synthesis time of 5 h and zeolite A produced with ultrasound for 10 min with a power of 30 W at a frequency of 40 kHz and a synthesis time of 3.5 h.

Sample	A_{BET} / m^2/g	V_{MP} / cm^3/g
5 h-NoUS	594.5	0.21
3.5 h-US-10 min-30 W	669.6	0.24

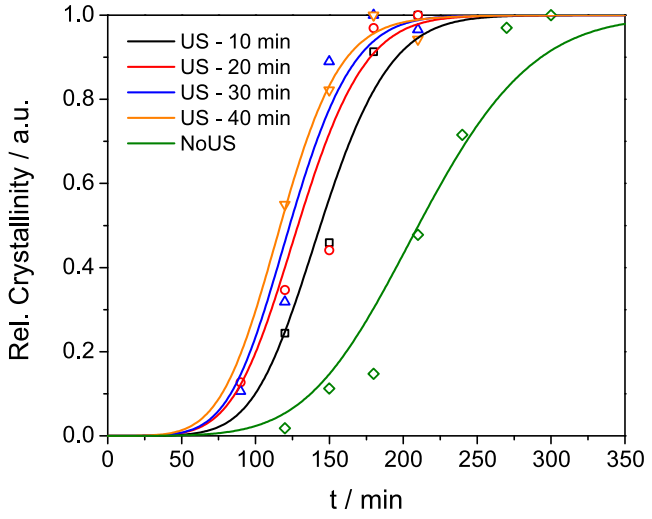

Fig. 8. Experimental and model data obtained by the model of Gualtieri for the crystallization curves of zeolite A synthesized at 80 °C without ultrasound and under sonicated conditions for 10 min, 20 min, 30 min and 40 min at 40 kHz and a sonication power of 33 W.

Table 5
Fitting data obtained by the model of Gualtieri with the experimental data for the zeolite A synthesis at 80 °C without ultrasound and sonication for 10 min, 20 min, 30 min and 40 min at 40 kHz and a sonication power of 33 W.

	NoUS	10 min	20 min	30 min	40 min
k_g / min^{-1}	0.0048	0.0071	0.0079	0.0082	0.0091
k_n / min^{-1}	0.0064	0.0086	0.0101	0.0106	0.0106
b / min	44.32	23.99	24.40	22.07	25.19
R^2	0.9452	0.9425	0.9891	0.9424	0.9642

major effects can be attributed to the increase of the growth rate constant. Acoustic streaming, which is the fluid motion introduced by the sound field applied [29], generates additional mixing. With the therefore improved mass transfer, the growth of zeolite A is accelerated. Additionally, the collapsing cavitation bubbles form local hot-spots [30–32]. Hence, growth kinetics are accelerated that lead to a faster formation of the crystalline zeolite. For the fitting parameter b no significant difference is present between the different sonication durations and an autocatalytic nucleation is predicted for all cases.

Comparing the particle size distributions in Fig. 9 of different sonication times, after a synthesis time of 3.5 h, shows slight differences depending on how long ultrasound is used. The d_{50}, shown in Table 6, decreases with an increased sonication time from 10 min to 30 min, after which an increase in size is measured again at 40 min of sonication. It appears that with the enhanced nucleation by ultrasound smaller particles are formed. Yet, as the crystallization process is further advanced with 40 min of sonication, due to the faster growth rate, larger particles are formed.

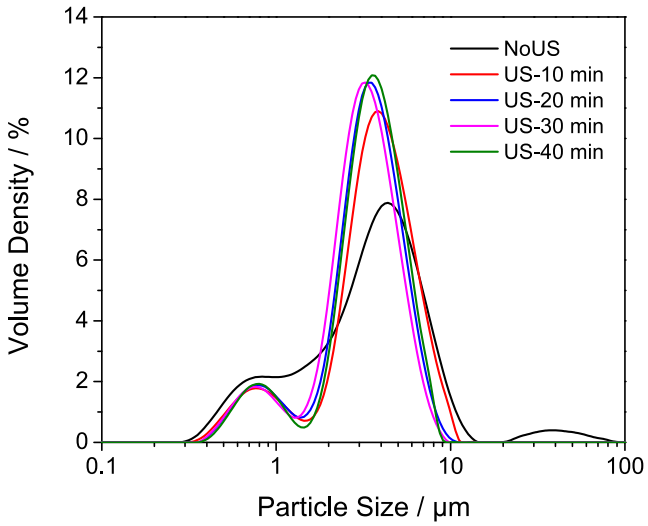

Fig. 9. Particle size distributions of zeolite A synthesized at 80 °C without ultrasound and sonication for 10 min, 20 min, 30 min and 40 min at 40 kHz and a sonication power of 33 W, for a fixed synthesis time of 3.5 h.

Table 6
Measured values for d_{10}, d_{50} and d_{90} for zeolite A synthesized at 80 °C without ultrasound and with sonication for 10 min, 20 min, 30 min and 40 min at 40 kHz and a sonication power of 33 W, for a fixed synthesis time of 3.5 h. Measurement errors are not shown, due to them being beyond the detection limit of the device.

t_{son} / min	d_{10} /µm	d_{50} /µm	d_{90} /µm
10	1.11	3.97	7.08
20	1.12	3.56	6.03
30	1.15	3.33	5.68
40	1.16	3.70	6.17

4. Conclusion

To investigate the effect of ultrasound on the synthesis of zeolite A, the kinetic model developed by Gualtieri was used to obtain an overview about the crystallization parameters. Different sonication powers were used at a fixed sonication time of 10 min where it was shown that an optimum power exists at 0.25 W/cm^3. Under those conditions the growth process was initiated the fastest and in total a reduction of required synthesis time by 30 % was achieved. Additionally, ultrasound affected the particle size distribution, where a more evenly distributed size was achieved, compared to zeolite A that is produced in silent conditions. Moreover, various sonication times were used in a range between 10–40 min. With increasing sonication time slight decreases in the required time to obtain fully crystalline zeolite A were observed. According to the model of Gualtieri the nucleation is influenced by ultrasound until a sonication time of 20 min. For longer sonication the main effect was predicted to be on the growth. In total, a further reduction to in total 40 % of the initial synthesis time of zeolite A can be achieved, by increasing the sonication time. In terms of particle size, an increase of sonication time leads to a reduction of the d_{50}, until a rise is observed for a sonication of 40 min. On the BET surface area ultrasound appears to have a beneficial effect by increasing the surface area by approximately 13 %, compared to zeolite A synthesized under conventional conditions. With the data obtained it is possible to optimize the synthesis conditions of zeolite A using ultrasound.

CRediT authorship contribution statement

Ruben M. Dewes: Conceptualization, Data curation, Formal analysis, Investigation, Methodology, Validation, Visualization, Writing –

original draft, Writing – review & editing. **Heidy Ramirez Mendoza:** Methodology, Resources, Writing – review & editing. **Mafalda Valdez Lancinha Pereira:** Methodology, Resources, Writing – review & editing. **Cécile Lutz:** Methodology, Resources, Writing – review & editing. **Tom Van Gerven:** Conceptualization, Funding acquisition, Methodology, Project administration, Supervision, Writing – review & editing.

Declaration of Competing Interest

The authors declare that they have no known competing financial interests or personal relationships that could have appeared to influence the work reported in this paper.

Acknowledgments

This project has received funding from the European Union's Horizon 2020 research and innovation programme under grant agreement No. 820716

References

[1] M.N. Hussain, J. Jordens, J.J. John, L. Braeken, T. Van Gerven, Enhancing pharmaceutical crystallization in a flow crystallizer with ultrasound: Anti-solvent crystallization, Ultrason. Sonochem. 59 (2019), 104743, https://doi.org/10.1016/j.ultsonch.2019.104743.

[2] M.N. Hussain, S. Baeten, J. Jordens, L. Braeken, T. Van Gerven, Process intensified anti-solvent crystallization of o-aminobenzoic acid via sonication and flow, Chem. Eng. Process.- Process Intensification 149 (2020), 107823, https://doi.org/10.1016/j.cep.2020.107823.

[3] J. Jordens, B. Gielen, L. Braeken, T. Van Gerven, Determination of the effect of the ultrasonic frequency on the cooling crystallization of paracetamol, Chem. Eng. Process. 84 (2014) 38–44, https://doi.org/10.1016/j.cep.2014.01.006.

[4] K. Wohlgemuth, A. Kordylla, F. Ruether, G. Schembecker, Experimental study of the effect of bubbles on nucleation during batch cooling crystallization, Chem. Eng. Sci. 64 (19) (2009) 4155–4163, https://doi.org/10.1016/j.ces.2009.06.041.

[5] L. d. l. S. Castillo–Peinado, M.D.L. d. Castro, The role of ultrasound in pharmaceutical production: sonocrystallization, Journal of Pharmacy and Pharmacology 68 (10) (2016) 1249–1267, _eprint: https://onlinelibrary.wiley.com/doi/pdf/10.1111/jphp.12614. doi:https://doi.org/10.1111/jphp.12614.

[6] J. Grand, H. Awala, S. Mintova, Mechanism of zeolites crystal growth: new findings and open questions, CrystEngComm 18 (5) (2016) 650–664, https://doi.org/10.1039/C5CE02286J.

[7] C.S. Cundy, P.A. Cox, The Hydrothermal Synthesis of Zeolites: History and Development from the Earliest Days to the Present Time, Chem. Rev. 103 (3) (2003) 663–702, https://doi.org/10.1021/cr020060i.

[8] T. Brar, P. France, P.G. Smirniotis, Control of Crystal Size and Distribution of Zeolite A, Ind. Eng. Chem. Res. 40 (4) (2001) 1133–1139, https://doi.org/10.1021/ie000748q.

[9] M. Itakura, I. Goto, A. Takahashi, T. Fujitani, Y. Ide, M. Sadakane, T. Sano, Synthesis of high-silica CHA type zeolite by interzeolite conversion of FAU type zeolite in the presence of seed crystals, Microporous Mesoporous Mater. 144 (1) (2011) 91–96, https://doi.org/10.1016/j.micromeso.2011.03.041.

[10] Y. Mu, Y. Zhang, J. Fan, C. Guo, Effect of ultrasound pretreatment on the hydrothermal synthesis of SSZ-13 zeolite, Ultrason. Sonochem. 38 (2017) 430–436, https://doi.org/10.1016/j.ultsonch.2017.03.043.

[11] H. Ramirez Mendoza, J. Jordens, M. Valdez Lancinha Pereira, C. Lutz, T. Van Gerven, Effects of ultrasonic irradiation on crystallization kinetics, morphological and structural properties of zeolite FAU, Ultrason. Sonochem. 64 (2020) 105010. doi:10.1016/j.ultsonch.2020.105010.

[12] Ö. Andaç, M. Tatlıer, A. Sirkecioğlu, I. Ece, A. Erdem-Şenatalar, Effects of ultrasound on zeolite A synthesis, Microporous Mesoporous Mater. 79 (1) (2005) 225–233, https://doi.org/10.1016/j.micromeso.2004.11.007.

[13] N. Jusoh, Y.F. Yeong, M. Mohamad, K.K. Lau, A.M. Shariff, Rapid-synthesis of zeolite T via sonochemical-assisted hydrothermal growth method, Ultrason. Sonochem. 34 (2017) 273–280, https://doi.org/10.1016/j.ultsonch.2016.05.033.

[14] B. Wang, J. Wu, Z.-Y. Yuan, N. Li, S. Xiang, Synthesis of MCM-22 zeolite by an ultrasonic-assisted aging procedure, Ultrason. Sonochem. 15 (4) (2008) 334–338, https://doi.org/10.1016/j.ultsonch.2007.07.007.

[15] T.Y.S. Ng, T.L. Chew, Y.F. Yeong, Z.A. Jawad, C.-D. Ho, Zeolite RHO Synthesis Accelerated by Ultrasonic Irradiation Treatment, Scientific Rep. 9 (1) (2019) 15062, https://doi.org/10.1038/s41598-019-51460-x.

[16] S. Askari, S. Miar Alipour, R. Halladj, M.H. Davood Abadi Farahani, Effects of ultrasound on the synthesis of zeolites: a review, J. Porous Mater. 20(1) (2013) 285–302. doi:10.1007/s10934-012-9598-6. url:https://doi.org/10.1007/s10934-012-9598-6.

[17] R.W. Thompson, M.J. Huber, Analysis of the growth of molecular sieve zeolite NaA in a batch precipitation system, J. Cryst. Growth 56 (3) (1982) 711–722, https://doi.org/10.1016/0022-0248(82)90056-2.

[18] A.F. Gualtieri, Synthesis of sodium zeolites from a natural halloysite, Phys. Chem. Miner. 28 (10) (2001) 719–728, https://doi.org/10.1007/s002690100197.

[19] B. Gielen, S. Marchal, J. Jordens, L.C.J. Thomassen, L. Braeken, T. Van Gerven, Influence of dissolved gases on sonochemistry and sonoluminescence in a flow reactor, Ultrason. Sonochem. 31 (2016) 463–472, https://doi.org/10.1016/j.ultsonch.2016.02.001.

[20] A. Barati, M. Mokhtari-Dizaji, H. Mozdarani, S.Z. Bathaie, Z.M. Hassan, Free hydroxyl radical dosimetry by using 1 MHz low level ultrasound waves, Iran. J. Rad. Res. 3 (2006) 163–169.

[21] A. Katovic, Crystallization of tetragonal (B8) and cubic (B1) modifications of zeolite NaP from freshly prepared gel. Part 1. Mechanism of the crystallization, Zeolites.

[22] M.M. van Iersel, N.E. Benes, J.T.F. Keurentjes, Importance of acoustic shielding in sonochemistry, Ultrason. Sonochem. 15 (4) (2008) 294–300, https://doi.org/10.1016/j.ultsonch.2007.09.015.

[23] P.R. Gogate, S. Mujumdar, A.B. Pandit, Sonochemical reactors for waste water treatment: comparison using formic acid degradation as a model reaction, Adv. Environ. Res. 7 (2) (2003) 283–299, https://doi.org/10.1016/S1093-0191(01)00133-2.

[24] S. Dähnke, F.J. Keil, Modeling of Three-Dimensional Linear Pressure Fields in Sonochemical Reactors with Homogeneous and Inhomogeneous Density Distributions of Cavitation Bubbles, Ind. Eng. Chem. Res. 37(3) (1998) 848–864, publisher: American Chemical Society. doi:10.1021/ie9703393.

[25] L.H. Thompson, L.K. Doraiswamy, Sonochemistry: Science and Engineering, Ind. Eng. Chem. Res. 38 (4) (1999) 1215–1249, https://doi.org/10.1021/ie9804172.

[26] J.J. John, J.P.G. d. Mussy, S. Kuhn, T.V. Gerven, The role of process intensification in the current business context of the chemical process industry, J. Adv. Manuf. Process. 3(3) (2021) e10086, _eprint: doi:10.1002/amp2.10086.

[27] G. Feng, P. Cheng, W. Yan, M. Boronat, X. Li, J.-H. Su, J. Wang, Y. Li, A. Corma, R. Xu, J. Yu, Accelerated crystallization of zeolites via hydroxyl free radicals, Science 351 (6278) (2016) 1188–1191, https://doi.org/10.1126/science.aaf1559.

[28] S. Mintova, N.H. Olson, V. Valtchev, T. Bein, Mechanism of Zeolite A Nanocrystal Growth from Colloids at Room Temperature, Science 283 (5404) (1999) 958–960, https://doi.org/10.1126/science.283.5404.958.

[29] S.J. Lighthill, Acoustic streaming, J. Sound Vib. 61 (3) (1978) 391–418, https://doi.org/10.1016/0022-460X(78)90388-7.

[30] K.S. Suslick, G.J. Price, Applications of ultrasound to materials chemistry, Annu. Rev. Mater. Sci. 29 (1) (1999) 295–326, https://doi.org/10.1146/annurev.matsci.29.1.295.

[31] J.J. Hinman, K.S. Suslick, Nanostructured Materials Synthesis Using Ultrasound, Top. Curr. Chem. 375 (1) (2017) 12, https://doi.org/10.1007/s41061-016-0100-9.

[32] L.H. Thompson, L.K. Doraiswamy, Sonochemistry: Science and Engineering, Ind. Eng. Chem. Res. 38 (4) (1999) 1215–1249, https://doi.org/10.1021/ie9804172.